Assessment of the PETase Conformational Changes Induced by Poly(ethylene terephthalate) Binding

Clauber Henrique Souza da Costa[1], Alberto M. dos Santos[2], Cláudio Nahum Alves[1], Sérgio Martí[3], Vicent Moliner[3,*], Kauê Santana[4,*], Jerônimo Lameira[5,*]

[1]*Institute of Natural Sciences. Federal University of Pará, 66075-110, Belém, Pará, Brazil.*

[2]*Centro de Ciências Exatas e Tecnologias. Federal University of Maranhão, 65080-805, São Luis, Maranhão, Brazil.*

[3]*Departamento de Química Físcia y Analítica,Universitat Jaume I, 12071 Castellón, Spain*

[4]*Institute of Biodiversity. Federal University of Western Pará, Santarém, Pará, Brazil.*

[5]*Institute of Biological Sciences. Federal University of Pará, 66075-110, Belém, Pará, Brazil*.

*Corresponding authors:

Jerônimo Lameira; Phone: +55 91 32018235; E-mail: lameira@ufpa.br

Kauê Santana. E-mail: kaue.costa@ufopa.edu.br

Vicent Moliner; Phone: +34 964728084; E-mail: moliner@uij.es

ORCID of the authors:

Clauber Henrique Souza da Costa: 0000-0002-6915-1056.

Alberto Monteiro dos Santos: 0000-0002-7033-3922.

Sergio Martí: 0000-0002-1087-7143.

Kauê Santana: 0000-0002-2735-8016.

Jerônimo Lameira: 0000-0001-7270-1517.

Vicent Moliner: 0000-0002-3665-3391.

Data availability statement

All data from the present study can be accessed in the supplementary material or requested via corresponding authors' e-mail.

Funding statement

The present study was supported by the Spanish Ministerio de Ciencia e Innovación (grant PGC2018-094852-B-C21), the Generalitat Valenciana (Grant AICO/2019/195) and Universitat Jaume I (grant UJI-B2020-03) and Conselho Nacional de Desenvolvimento Científico e Tecnológico (CNPq, Brazil) and Coordenação de Aperfeiçoamento de Pessoal de Nível Superior (CAPES, grant number: 88882.466102/2019-01 and 88887.599350/2021-00).

Conflict of interest statement

The authors declare no conflict of interest regarding the publication of the manuscript. The funders had no role in the design of the study; in the collection, analyses, or interpretation of data; in the writing of the manuscript, or in the decision to publish the results.

Authors contribution statement

Conceptualization: S.M, V.M., K.S., and J. L.; investigation: C.H.S.C and A.M.S; data curation: S.M, V.M., C.N.A, and K.S.; writing—original draft preparation, S.M, V.M., K.S., J. L.; writing—review and editing: A.M.S, C.N.A, S.M, V.M., K.S., and J. L supervision: S.M, V.M., K.S., and J. L. All authors have read and agreed to the published version of the manuscript.

Abstract

Recently, a bacterium strain of *Ideonella sakaiensis* was identified with the uncommon ability to degrade the poly(ethylene terephthalate) (PET). The PETase from *I. sakaiensis* strain 201-F6 catalyzes the hydrolysis of PET converting it to mono(2-hydroxyethyl) terephthalic acid (MHET), bis(2-hydroxyethyl)-TPA (BHET), and terephthalic acid (TPA). Despite the potential of this enzyme for mitigation or elimination of environmental contaminants, one of the limitations of the use of PETase for PET degradation is the fact that it acts only at moderate temperature due to its low thermal stability. Besides, molecular details of the main interaction of PET in the active site of PETase remain unclear. Herein, molecular docking and molecular dynamics (MD) simulations were applied to analyze structural changes of PETase induced by PET binding. Results from the essential dynamics revealed that the β1-β2 connecting loop is very flexible. This Loop is located far from the active site of PETase and we suggest that it can be considered for mutagenesis to increase the thermal stability of PETase. The free energy landscape (FEL) demonstrates that the main change in the transition between the unbounded to the bounded state is associated with the β7-α5 connecting loop, where the catalytic residue Asp206 is located. Overall, the present study provides insights into the molecular binding mechanism of PET into the PETase structure and a computational strategy for mapping flexible regions of this enzyme, which can be useful for the engineering of more efficient enzymes for recycling the plastic polymers using biological systems.

Keywords: plastic, environmental biotechnology, PETase, catalysis, molecular dynamics, principal component analysis.

Introduction

Synthetic polymers, such as poly(ethylene terephthalate) (PET) revolutionized modern human civilization due to their versatile applications and low-cost production. However, due to the ultralong lifetimes of most PET-based plastic waste and the high resistance to biodegradation[1,2], these synthetic polymers remain one of the most challenging environmental problems with serious impacts on ecosystems and biodiversity [3–5].

Ideonella sakaiensis strain 201-F6 was recently discovered with the unusual ability to degrade and use synthetic polymers, such as PET, as its major energy and carbon source [6]. This discovery opened up new scientific researches to find a solution for plastic waste using environmentally friendly alternatives based on enzymatic recycling in mesophilic temperatures [7–10].

Yoshida group demonstrated that *I. sakaiensis* express two closely related enzymes involved with the PET degradation [6,11]. The first enzyme is named PETase (PET-digesting enzyme), which converts PET to mono(2-hydroxyethyl) terephthalic acid (MHET), bis(2-hydroxyethyl)-TPA (BHET), and terephthalic acid (TPA) as products. The second enzyme is the MHETase (MHET-digesting enzyme) that further converts MHET into two monomers: ethylene glycol (EG) and TPA [12]. Structural and evolutionary studies of PETase have shown that its structure resembles that of α/β-hydrolase enzymes [13]. The α/β-hydrolase family includes lipases and cutinases, which catalyze the hydrolysis of fatty acids and cutin, respectively [13–15].

The PET-hydrolyzing enzymes were reported to be expressed in several organisms including fungi [16–19] and bacteria [20–22] that usually inhabit environments containing plastic debris or organic matters. However, although several structures of these enzymes have been reported recently, only a few of them are

complexed with the PET polymer or its analogs [13,22–26]. Thus, the PET-binding mode has been predicted mostly through computational methods [22,27].

The PETase binding site is larger when compared to thermostable cutinases, and also contains large hydrophobic residues, such as Trp156, important for substrate stabilization [13,28]. Additionally, the PETase backbone does not show high conformational changes when bound to PET and the movements have been described as limited to the binding subsite [14,28].

Several studies have proposed a molecular mechanism for enzymatic catalysis [14,28,29]. The conserved catalytic triad Ser160, Asp206, and His237 is present in the active site of the PETase [13,14] and shares the same spatial orientation of α/β hydrolases enzymes. Fig 1 shows the PETase secondary and tertiary structures (PDB code: 6EQE), with its typical α/β-hydrolase fold containing two disulfide bonds (Cys203-Cys239 and Cys273-Cys289), which guarantee an extra rigidity to the protein structure, and 7 α-helices (α.1 - α.7), 9 β-sheets (β.1 - β.9), and 14 loops.

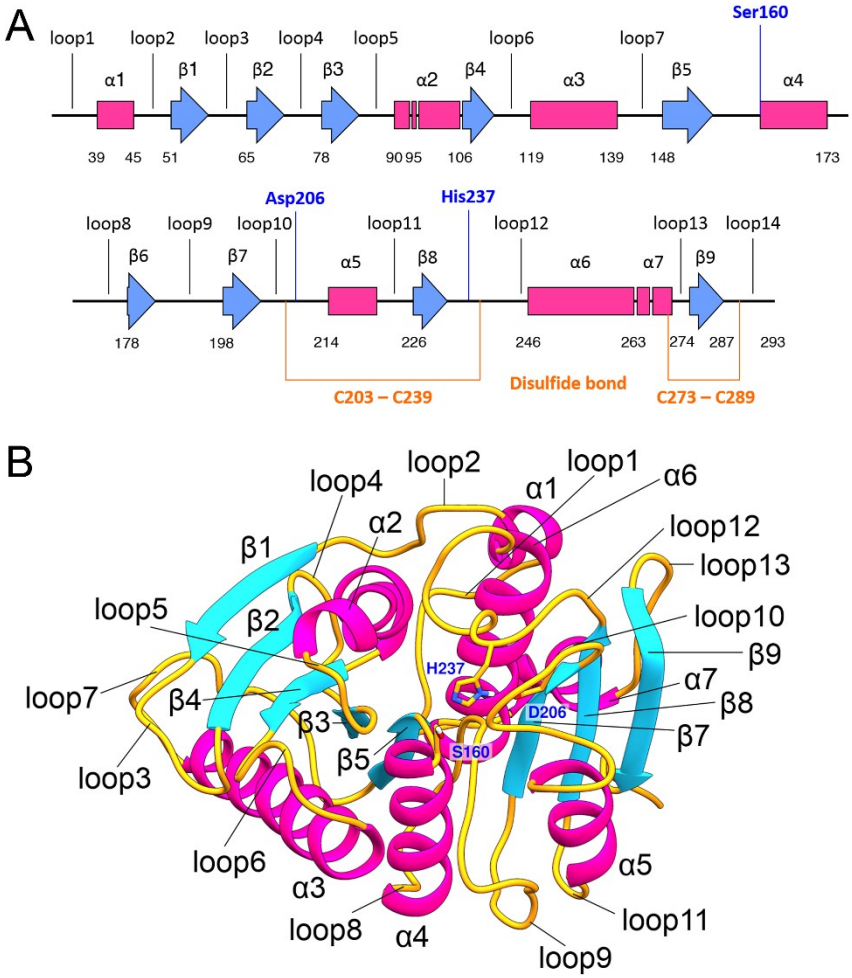

95

96 **Fig 1**. **Schematic overview of the PETase structure of *I. sakaiensis*.** (A) The
97 secondary structure of PETase with catalytic residues highlighted in blue and disulfides
98 bonds of the cysteines in orange (B) Tertiary structure of PETase with the catalytic
99 residues highlighted in blue.

100 In the active site, a disulfide bond between the residues Cys176 and Cys212 is
101 related to thermal stability [15]. Moreover, the reduction of these cysteines results in a
102 dramatic increase in the structural flexibility of the active site, thus destabilizing the
103 integrity of the catalytic triad, which leads, consequently, to a decrease of the enzymatic
104 activity [15]. Despite its remarkable activity in the catalyze of PET polymers, the wild-
105 type structure of the PETase is not optimized for full degradation of PET, and details of
106 the catalytic mechanism of this reaction remain unknown [24].

One of the limitations of the use of PETase for PET degradation is the fact that it acts only at mild temperatures due to its low thermal stability. Therefore, the thermal stability of PETase may be crucial for effective PET degradation using this enzyme. Recently, Son and coworkers have increased the thermal stability of the PETase from *I. sakaiensis* variants with remarkably enhanced thermal stability and highly improved PET degradation ability.[9] They have used the B-factor value as a parameter to map flexible regions of the protein far from the active site. Then, they explored some point mutations to increase the stability of the protein structure. Son and coworkers [9] found that the β6-β7 connecting loop was a flexible region based on B-factor value and it was used as a target region of the protein for mutation. Indeed, point mutations have been used for stabilizing protein structure and the substitutions are proposed in flexible regions of the protein-like loops [30]. Recently, Cui et al have successfully redesign PETase from Ideonella sakaiensis to improve its robustness using a systematic clustering analysis combined with the greedy accumulation of beneficial mutations in a computationally derived library [31]. In this work, we have examined in detail the protein conformational changes and residue fluctuations using essential dynamics to suggest for mutagenesis potential target regions of PETase. In addition, we have explored the binding mode of PET into the PETase subsites using computational approaches. Currently, the binding mode of PET into the PETase subsites is not fully elucidated due to difficulties in co-crystallization and low solubility of the entire polymer [13,14]. Our computational results could shed light on further studies that aim to engineer its structure, to determine and improve its activity for the recycling of plastic polymers using biological systems.

Material and Methods

Molecular Docking

The binding mode of PET in the PETase structure is unknown, thus we performed molecular docking of an oligomer consisting of four monomers in their low free-energy conformations to analyze the selectivity and affinity of the polymer during the initial stages of the PETase catalytic process. Considering the wild-type structure of *I. sakaiensis* PETase (PDB: 6EQE, X-ray diffraction with 0.92 Å resolution) was the first reported enzyme with affinity and catalytic activity against the PET[24], we choose this structure with high resolution as a target to perform a detailed analysis of the interatomic interactions established between the protein and the PET. Note that we have used molecular docking to obtain the PETase-PET complex.

To perform the molecular docking against the PETase binding subsites, we used the AutoDock Vina (version 1.1.2) [32] program with the following forms mimicking PET: monomer (bis-(hydroxyethyl) terephthalate, BHET), dimer (2-hydroxyethyl-(mono-hydroxyethyl terephthalate)$_2$, 2-HE(MHET)$_2$), and tetramer (2-hydroxyethyl-(mono-hydroxyethyl terephthalate)$_4$, 2-HE(MHET)$_2$) [13]. Conjecturing that the conformation of the PET tetramer in the PETase corresponds to that of individual monomers bound at PETase subsites I to IV, we sequentially constructed 3 models of PET: Model I comprises the individual PET monomers against four proposed binding subsites of PETase. In Model II), we combined two PET monomers, thus forming a dimer to dock against two adjacent PETase binding subsites. In Model III, we joined the four PET monomers forming a tetramer to dock against four potential adjacent PETase binding subsites (subsites I to IV). Table S1 shows the parameters used in the docking of the three models of PET

The molecular docking in the AutoDock Vina was performed considering the flexibility of the residues from the subsites (Tyr87, Trp159, Ser160, Met161, Ile208, Asn233, His 237, Ser238, Asn241, and Arg280), as well as the flexibility of the ligand. The following Cartesian coordinates of the center of the docking grid, in Å, were applied: X = -0.51, Y = 4.23, and Z = 20.09; with dimensions of x = 70, y = 56, and z = 68 for PET flexible docking.

Further validation was performed using Molegro Virtual Docker (MVD) [33] and CSD-GOLD [34]; then compared with the conformations obtained by the AutoDock Vina (available in Table S1 and Table S3). After analysis and validation, the top-predicted pose of Audodock Vina PETase-PET complex was used as the starting point for the MD simulations.

Molecular Dynamics Simulations

To evaluate the conformational dynamics of the PETase, we performed MD simulations in the Amber16 package [35] with structures derived from the docking study. The structure of PETase has two disulfide bonds (203-239 and 273-289) that play an important role in maintaining and stabilizing the protein structure. We performed MD simulations for two PETase systems: PETase in the unbounded state (system I); and PETase in complex with PET tetramer (2-HE(MHET)$_4$) (system II). The simulation of polymers may be particularly difficult [36,37]. Therefore, to obtain a satisfactory sampling of the PETase in the bounded state, we applied restraint forces. This approach has been useful to identify domain motions especially for those of computational challenging systems [38,39]. Nevertheless, a system of PETase complexed with PET without constraint forces in the ligand complexed in the binding pocket (system III) was also explored.

First, the residues of protein were treated with the ff99SB force field [40]. The restrained electrostatic potential (RESP) protocol was used to calculate the charges of PET tetramer using the Gaussian09 program [41] with the Hartree-Fock method and the 6-31G* base set according to Amber protocol. The charges were then obtained using the antechamber module available in the Amber16 package. To describe PET complexed with PETase, the ligand was treated with the general Amber force field and the receptor (PETase enzyme) was treated with Amber FF99SB forcefield. Both systems were solvated in an octahedral periodic box of 12 Å side, with the TIP3P water solvation model [42]. The systems were neutralized with Cl^- ions to avoid unbalanced charges. The resulting systems were solvated with TIP3P water, where it was applied octahedral periodic boundary conditions. All stages simulations employed a nonbonded cutoff of 8 Å, where particle mesh Ewald (PME) approach computed the long-range Coulomb forces.

Prior to the MD simulation, the water molecules, ions, PETase structure were minimized with 7 steps with 10,000 cycles of steepest descent and conjugate gradient algorithm to avoid clashes or improper geometries. We started the minimization with a constraint force equal to 500 $kcal.mol^{-1} \cdot Å^{-2}$ applied in the cartesian coordinates, which was gradually decreased during minimization to relax the waters, counterions, protein, and ligand structure. Afterward, the systems were heated in 10 steps from 0 to 300K. The 1st heating step was maintained at constant volume during 20ps (0 to 100K), from the 2nd to the 9th step the temperature was gradually increased from 25 to 25k until reaching 275 K with each step performed in a time of 1 ns for each step, and in the 10th step (last heating step) the system reached the temperature of 300K. Then, we performed 5 ns of MD simulation to balance the density of the system and maintain a constant pressure (1 bar) and temperature (300K). Here, we maintained the PET tetramer interacting with the PETase binding sites (I to IV) using a restraint force of 150

kcal.mol^{-1}·Å^{-2} on the Cartesian coordinates of PET obtained from molecular docking. The SHAKE algorithm was applied for all hydrogen bonds in the analyzed systems. It is worth noting that restraint forces in the ligand structures in complex with the molecular receptor are widely applied to allow the conformational adaptation of the receptor structure to the ligands, thus, establishing favorable intermolecular interaction [43,44]. It is important to highlight that the restraints force also increases the conformational stability of the complex throughout the MD simulation, avoiding the loss of the interaction between the investigated structures, and misinterpretation of the binding free energy values [45,46].

In the production stage of the unbounded and bounded systems (systems I and II), we performed 500ns of MD simulations for each system using the NPT ensemble, and each system was replicated and assigned with different initial velocities to generate independent simulations.

Principal Component Analysis (PCA) and Free Energy Landscape (FEL)

The PCA is a technique that allows to reduces the dimensions of the analyzed trajectories during the MD simulation of the covariance matrix (C), thus reducing the linear correlations between the spatial coordinates and converting them into a set of an orthogonal vector named principal component (PC) which describes the movements using the Cartesian coordinates X, Y, and Z of each analyzed atom [47]. This technique has been widely combined with MD simulations to evaluate the conformational changes of protein structures [39,48–53]. Here, the CPPTRAJ module available in the Amber16 package was used to obtain the trajectories of PETase structures using the Cα coordinates over the 500ns of MDs to generate the principal components (PC1, PC2,

and PC3). The principal components that represent the protein movement are described according to Equation 1 [54–56]:

$$C_{ij} = \langle q_i q_j \rangle = \frac{1}{K} \sum_{k=1}^{K} q_i^k q_j^k \qquad (1)$$

Where K is the configuration stored during an equilibrated MD simulation and q_i^k , as defined in Equation 2, is the internal mass-displacement of Cartesian coordinates x_i^k from *i* atom (*i*= 1,..., N; N = number of atoms from the molecule) with mass m_i, and the angular support represents the average obtained from the *K* configurations from the MD simulation after the equilibration[54].

$$q_i^k = \sqrt{m_i} \left(x_i^k - \langle x_i \rangle \right) \qquad (2)$$

The diagonalization of the 3N × 3N covariance matrix C could be calculated (Equation 3):

$$\Lambda = L^T C L \qquad (3)$$

Where Λ is the diagonal matrix, which represents the relative contribution of each PC and contains the eigenvector, and L describes the matrix which contains the 3N orthonormal eigenvector Q_i. The eigenvalues show the mean square displacements (MSD) of Cα atoms, throughout the used eigenvectors, which describe the collective movement of protein [54–56]; and the diagonalization generates a reduced matrix with PC1, PC2, and PC3 for each frame obtained in MD simulation.

In the present study, we used the Bio3D package [57] to perform the principal component analysis (PCA). Herein, the PCs were obtained from the diagonalization of the covariance matrix obtained from the Cartesian coordinates of the superposed Cα

atoms of PETase structure. To avoid an underestimate of the atomic displacement, an iterated superposition procedure was applied before the PCA, where residues displaying the largest positional differences were excluded at each round until only the invariant 'core' residues remained [57].

The analysis of the free energy landscape (FEL) was performed using the PC1 and PC2 using the terms of Equation 4:

$$\Delta G\left(PC_s\right) = -k_B T\left[ln\rho\left(PC_1, PC_2\right) - \ln \rho_{max}\right] \qquad (4)$$

The Gibbs free energy involving the principal components PC1 and PC2 is referred to as $\Delta G\left(PC_s\right)$, which is in the function of the probability distribution obtained from the MD trajectories, k_B is the Boltzmann constant, T is the temperature, ρ_{max} is the probability of maximum value subtracted from the free energy value, contained in the most significant conformation, to approximate it to zero [58,59]. To explore the conformations that are close to the native structure, the FEL values represented in two-dimensional were obtained from both probability distributions of PC1 and PC2 for all analyzed systems. To obtain the FEL plot and the conformational states of the PETase structure in the minimum of the energy landscape, we used the CPPTRAJ module of the Amber16 package. It is important to note that PCs were used to recognize the main structures that compose the first movement (PC1) and the second movement (PC2). We only considered the atomic coordinates of the bounded and unbounded states of PETase structure to obtain the PCA plots to ensure the same amount of the analyzed atoms.

Results and Discussion

In the present study, molecular docking and MD simulations were employed to provide information on the structural conformations and movements of PETase induced by the PET binding, as well as the selectivity and affinity of the substrate complexed with the PETase binding subsites.

Fig 2 shows the molecular docking obtained using the conformational search strategy of the monomers in the four PETase subsites based on previous studies [12,23], as described in the methods section. Our docking analysis demonstrated that the carbonyl oxygen of the PET ester group is positioned close to the nitrogen of the backbone amide group of the oxyanion hole (Fig 2). Fig 2A shows the binding mode of the four PET monomers analyzed separately, where the positioning of the monomer 1 (MHET moiety) formed π-π interactions with the aromatic amino acid Trp185 at the subsite (Fig S1), which were also observed previously observed by Han et al. 2017 [14]. The interaction distance between the Ser160 and the PET carbonyl is 5.88 Å. Panel B shows that the poses obtained for the dimers 1-2 and dimers 3-4 (Fig 2B) are similar to the individual monomers complexed at their respective subsites.

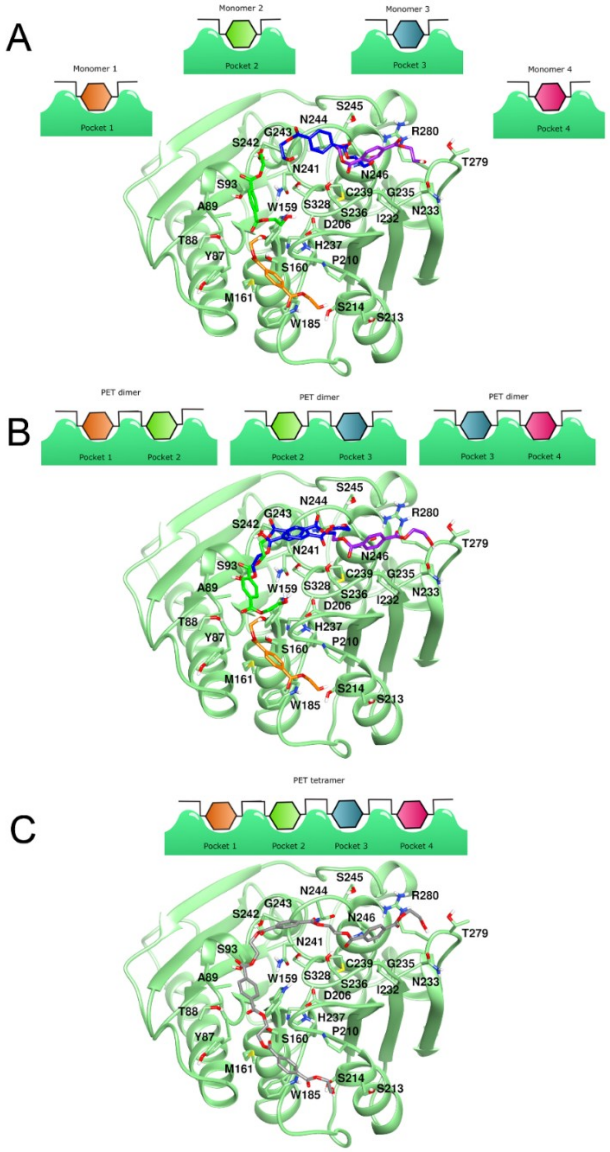

284

285 **Fig 2. Overview of the conformational search strategy applied in the**
286 **docking simulations.** (A) Docking of individual monomers in proposed binding regions
287 (B) Docking of dimers (C) Docking of the complete tetramer.

288 The following interatomic distances of the PETase catalytic triad were found:
289 between the oxygen (OG) from Ser160 and the nitrogen (NE2) from His237 was equal
290 to 3.19 Å, and between the ND1 from His237 and OD2 from Asp206 was equal to 2.75
291 Å. Also, the results of the molecular docking showed intermolecular interactions via
292 hydrogen bond of PET monomer 1 to the Ser213 (distance of 2.98 Å), monomer 4 to the
293 Ser236 (distance of 2.07 Å), and Thr279 (distance of 2.85 Å). Ala209 and Trp185 have

interesting interactions with monomer1, Ala209 showed a π-Alkyl interaction to the ring of monomer1, while Trp185 showed π- π interaction to the monomer1, showing an important role in the polymer positioning at the binding site during catalysis. The residues Ser214, Ile208, Pro210, Met161, His237, Asn241, Ser238, Cys239, Asn244, Gly235, Asn246, Ile232, Asn233, and Arg280 showed van der Waals interactions along with the PET polymer. Some molecular interactions are shown in Fig. S1.

The structure obtained from the molecular docking also showed a similar binding mode to the PETase crystallographic structure in complex with MHET (PDB ID: 5XH3) [14]. Thus, indicating a satisfactory docking result for the subsite I. Detailed comparison between the *pose* obtained from the molecular docking and the BHET binding mode in the PETase crystallographic structure is shown in Fig S2.

Fig 3 shows the electrostatic potential map of the crystallographic structure [24] used as a start point for the molecular docking simulation, where the highlighted region indicates the PET binding cavity (Fig 3A). The main residues for each subsite obtained by our docking results are shown in Fig 3B. The PETase subsites I-IV are proposed to accommodate four MHET moieties of the PET in an L shape (Fig 3B and 3C). The complex is stabilized mainly by hydrophobic interactions. Hydrogen bond interactions with Ser236 and Asn246 were observed at the ester linkages between the MHET moieties. The residue Arg280 also participated in the interaction at subsite IV (Fig 3C), although it is demonstrated that its absence showed much greater PET degradation activity [14]. Intermolecular distances between the atoms of the catalytic pocket and PET structure obtained from the molecular docking could be seen in Table S4.

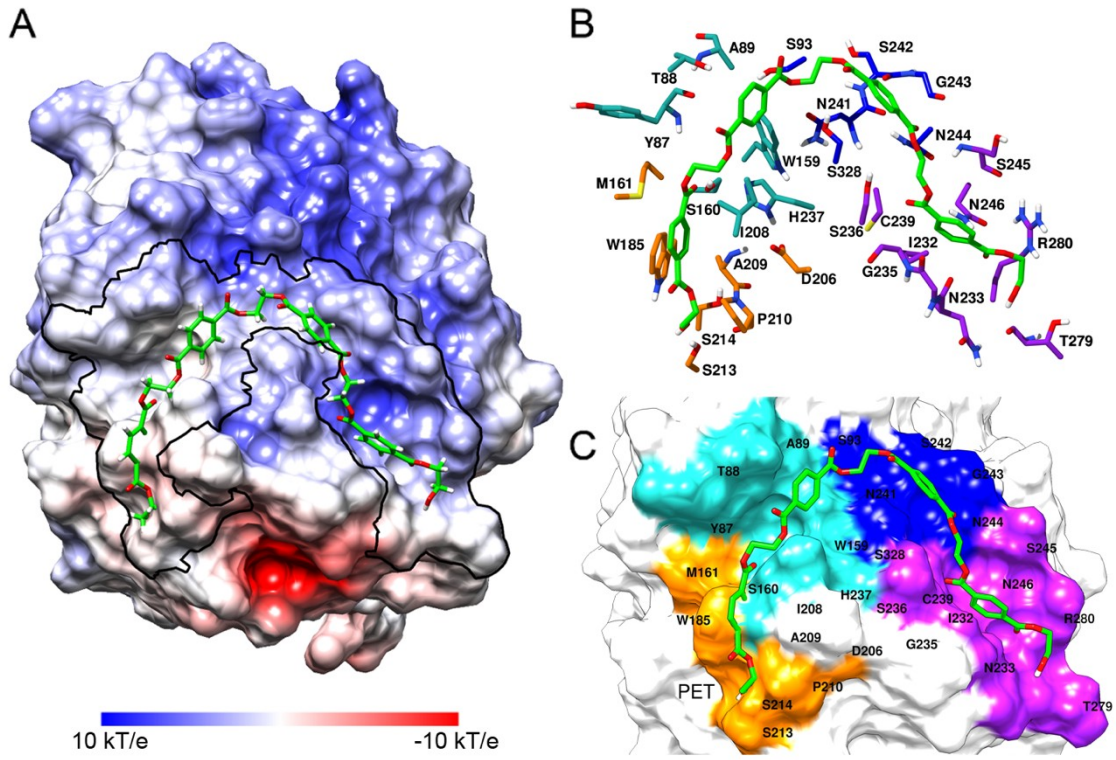

316

317 **Fig 3. Binding mode of PET complexed with PETase and the molecular**
318 **interactions obtained by the molecular docking simulations.** (A) Potential surface
319 map for the crystallographic protein, where the highlighted region indicates the
320 complete PET binding cavity (B) Residues belonging to the PETase binding subsites.
321 (C) Highlighted regions of each potential PETase binding site. Monomer 1 and subsite I
322 in orange; monomer 2 and subsite II in green; monomer 3 and subsite III in blue;
323 monomer 4 and subsite IV in purple.

324 The obtained binding modes (Fig 2C) demonstrated that the PET tends to fill the
325 same spatial regions of the subsites as a monomer, dimer, or tetramer. Therefore, our
326 PETase-PET complex represents a consistent and reliable model with favorable binding
327 energies. The pocket mapping was compared with the docking results obtained from
328 MVD [33] and GOLD [34] programs to validate our conformational search (see more in
329 Supporting information, Table S2).

330

Analysis of Molecular Dynamics of PETase

Our model for the PETase-PET complex started with a consistent binding mode as previously proposed in docking studies[13,24]. However, none of them considered the protein dynamics over time to analyze conformational changes in PETase structure, as well as conformational changes of PET complexed with the subsites. In this work, we used MD simulations to explore the conformational change of PETase upon PET binding. The RMSD plots of the PETase structure in the unbounded and bounded states are shown in Fig S3. Our MD simulations protocol successfully sampled the difficult-to-access configurations of the PETase structure in complex with PET, showing high stability during the MD simulation, with deviations below 3.0 Å (Fig S3 A). In general, the PETase in both bounded and unbounded states show no significant atomic RMSD deviation over the MD trajectory with RMSD values of 1.93 ± 0.43 Å and 1.56 ± 0.35 Å, respectively (Fig S3 B, and Table S5). Thus, further analysis to better describes the differences between the unbounded and bounded systems was carried out using more detailed analysis.

The analysis of the binding mode of PET complexed with PETase showed that the Trp159 from the subsite II formed a π-π stacking interaction with the aromatic ring from the MHET moiety (Fig S1). In addition, the Ile209 formed a π-alkyl interaction with the same structural moiety of PET located at the subsite II. Regarding subsite I, we noted that residue Trp186 (NE1) formed H-bond interactions with the oxygen atoms of the MHET moiety (O11, O13, and O14). We conjecture that these interactions are responsible to maintain the PET in subsite I and II over the MD trajectory. Differently, the subsites III and IV, the structural moieties of PET formed numerous hydrophobic contacts that weakly maintain the PET structure in the pocket. Thus, its structure suffers

considerable conformational changes that lead to its departure from the cavity. Fig S4 shows an overview of each MHET moieties (hexagons) complexed at their respective binding subsite during MD simulations.

Monomer 2 showed the most stable interactions in the elected binding subsites (system II, FigS5). In contrast, the monomers located at the extremities of the PET polymer (monomers 1 and 4) showed higher mobility. The RMSD plot also showed that the use of a restraint force to maintain the PET in the binding subsite allowed protein adjustments for a better fit during the first frames of the MD trajectory. When the restraint force was reduced, the PET conformation was gradually adjusted and remained in the subsite until the end of the 500ns of simulation.

We also analyzed the root-mean-square fluctuation (RSMF) for individual amino acid residue over the 500 ns of MD simulation. This analysis was used as a criterion for quantifying the flexibility of PETase, where higher RMSF values correspond to more flexible regions of the protein during MD simulation. The RMSF shows that the catalytic residues Asp206 and His237 located at β7-α5 and β8-α6 connecting loop, respectively, presented considerable mobility during MD simulations.

Essential Dynamics of PETase

As already commented in the Introduction section, the use of PETase for PET degradation is limited due to its low thermal stability. Thus, we have used essential dynamics to identify the flexible regions in the protein structure. These flexible regions in the PETase can be used as a potential target for enhancing thermal stability. Besides, this analysis can also provide insight into the induced-substrate conformational change in PETase. Herein, we performed a PCA for the two analyzed systems: (1) PETase in the unbounded state (ligand-free), and (2) PETase in the bounded state.

In accordance with PCA results, the residue Trp185 showed a considerable fluctuation between unbounded and bounded states (Fig 4). Curiously, the characteristic of the conformational movements of the Trp185 is directly related to the accessibility of the PET polymer since its fluctuation modifies the cavity and adjusts the monomer 1 accommodation at the binding site. Also, the movement of Trp185 possibly controls the subsite entrance of a new PET monomer in the binding subsite, thus leading to continuous depolymerization [24]. Moreover, during the MD simulation, the Trp 185 showed different conformations that increase the volume of the monomer 1 cavity to accommodate the polymer (Fig S5 and Fig S7), as previously observed [24].

These variations indicate that the protein alters its conformation to receive the substrate. It also indicates that Trp185 is involved in the permanence of the PET monomer in the first binding subsite of the enzyme as previously proposed [14]. In the bounded state (Fig S8), the Trp185 residue position, as well as all the catalytic residues of the protein, remained stable. This behavior could be associated with the catalytic residues exerting significant interactions with the ligand.

However, the permanence of PET in the binding subsite may impose local structure fluctuation, particularly, on the residue Trp185. This behavior was also observed for Ser160, the main catalytic residue. Moreover, the interaction of PET tetramer in the binding subsite causes a displacement of the residue Asp206 located at β7-α5 connecting loop. Conformational changes can play a crucial role in regulating the PET binding to the hydrophobic subsites and in the control of the catalysis. We noticed in the PCA analysis that the residues Asp206 and Trp185 are very flexible. The results also show considerable fluctuations in the residue His237 at β8-α6 connecting loop. Then, we conjecture that these residues are key residues for the mechanism of binding and release of PET.

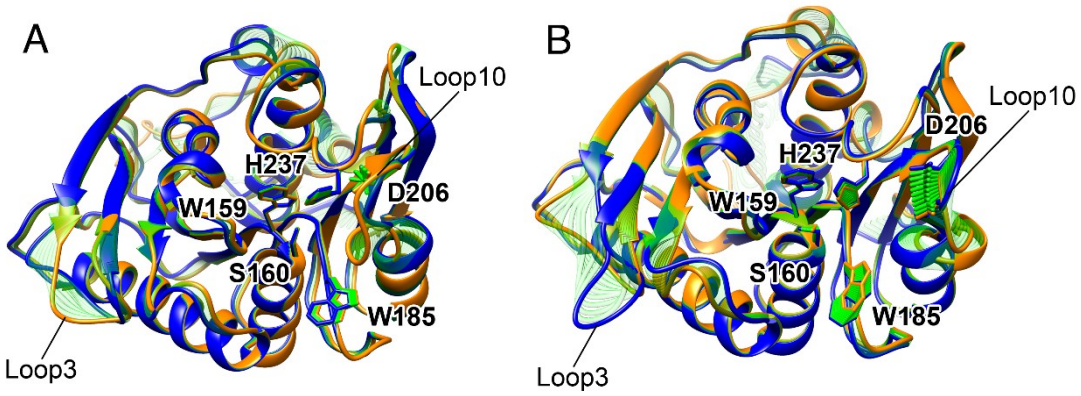

Figure 4. Essential motion described by the first principal component (PC1) of each analyzed PETase structure: A) PETase in the unbounded state, B) PETase in the bounded state. Loop3 and Loop10 corresponding to β1-β2 and β7-α5 connecting loops, respectively. The essential dynamics were obtained from 500 ns of MD simulations.

PCA result also shows that the most flexible region of the protein is located at β1-β2 connecting loops for both systems PETase in the unbounded and in the bounded state (Fig 4). It is worth noting that these essential dynamics involve almost 37.8% and 25.6 % of the motion of the unbounded and in the bounded systems, respectively (see SI). The results also reveal that participation in the conformational flexibility of β7-α5 and β1-β2 connecting loop is higher in PET-PETase complex than in PETase without ligand. Therefore, we suggest that the β1-β2 connecting loop may be targeted for mutagenesis to increase the PETase stability since it is located far from the active site.

Free Energy Landscape Analysis of PETase

As commented in the Introduction section, experimental works have suggested the PETase backbone does not present high conformational changes upon PET binding, since its movement is limited to the binding subsite [14,28]. Indeed, our PCA results show that the main movement of PETase is associated with β7-α5 and β1-β2

connecting loops motion. Since PCA describes the largest amplitude protein motions during a simulation, the bi-dimensional free energy landscape (FEL) was obtained taking into consideration the bidimensional projections of PC1 vs. PC2, which are considered the coordinates used for obtaining the FEL. The free energy landscape of PETase in the unbounded state shows that at the beginning of the MD, the conformations acquired by the PETase structure are similar to those obtained at the end of the simulation, thus demonstrating that conformational states of the PETase are not altered dramatically over the MD trajectory, which is in agreement with previous experimental data [14,28]. We also observed for the analysis of the $PCA_{PC2vsPC3}$ and $PCA_{PC1vsPC3}$ plots, a conformational dispersion at the end of MD simulation that not formed isolated clusters. It is important to note that the conformations of the PC1 were not directly correlated with those found in PC3, thus demonstrating that the initial structures are grouped separately from the other conformations that do not contain the PET at the binding site (see Fig S9).

The main difference between the most stable structure of PET-PETase complex (P1 in Fig 5) and unbound PETase (P6 in Fig 5) is in the β7-α5 connecting loop, where we noted that the Asp206 opened the cavity of the active site. Other conformational states with high probability were described for the unbounded state with P2 with a reduced cavity and P3 with an opened cavity similar to that of P1 (Fig 5A). Considering that the structural engineering of PETase using site-direct mutagenesis has led to optimized catalysis of PET [13,25,60], finding the most stable conformation of its structure is an important task for the improvement of its active site selectivity and also to better understand the conformational mechanism of the enzyme that influences in the catalysis.

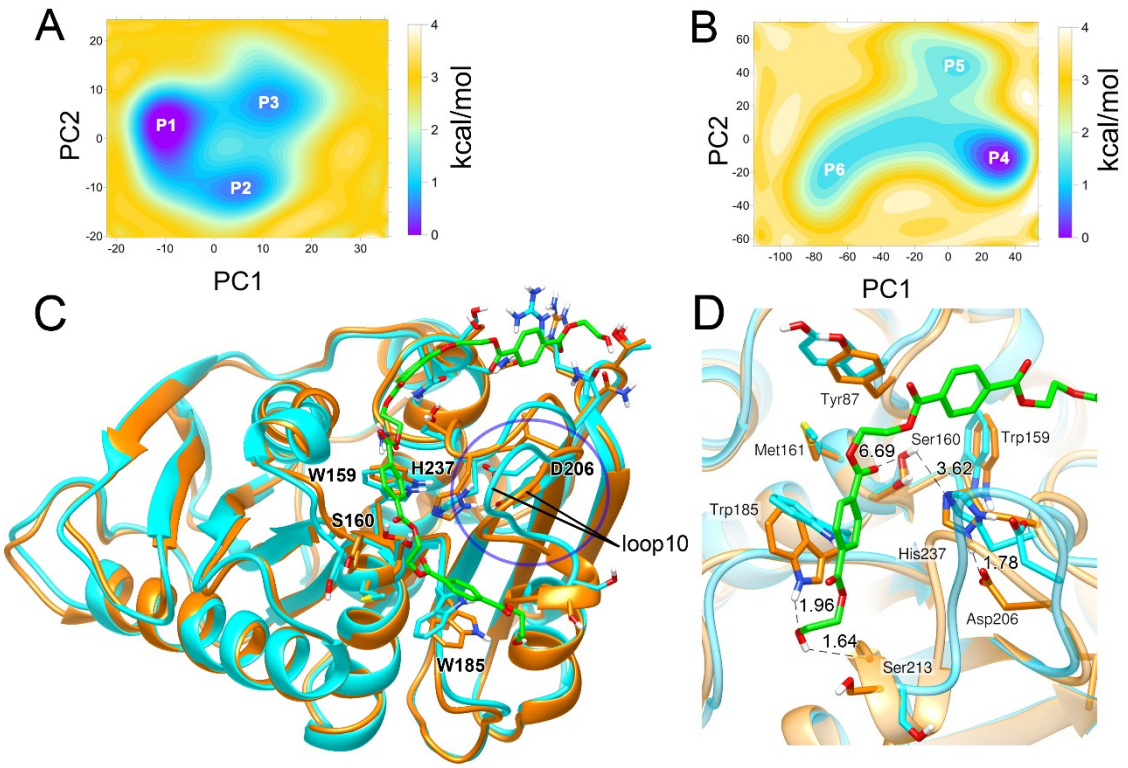

Fig 5. FEL analysis of different PETase systems (P1 vs P4) in their native conformations. (A) FEL of unbounded state (B) FEL of the bounded state. (C) Structural comparison between the minimal structures of PETase in the unbounded state (P1, blue) and the PETase in the bounded state (P4, orange) complexed with PET (green). The blue circle indicates the main conformational change between the two PETase states. The β7-α5 connecting loop is represented by Loop10.

The PETase has large regions with polar surface charges with few regions with acidic residues (red surfaces, Fig S10). In the subsite of monomer 1, more neutral regions are observed, while for the other monomers regions high hydrophobic surfaces are detected. There is an increase of the cavity's volumes (see SI) of the subsites when the PET structure is complexed to accommodate the PET, demonstrating conformational conservation of the catalytic triad. It is important to point out that the wide cleft in the active site would be necessary to accommodate semi-aromatic crystalline polyesters [24]. Recently, Knott and coworkers studied the catalytic

mechanism of the MHETase enzyme converting MHET to terephthalic acid and ethylene glycol.[61] The authors demonstrated that the main domain of MHETase is similar in the residue composition to PETase, which suggests insights into the hydrolysis mechanism of PET performed by the PETase [61]. However, the mobility of key residues and loops during the binding and catalysis remains unclear. Our analyzes of FEL revealed an increase in PETase stiffness upon binding of PET, which suggests that binding of PET gives rise to an effective motion of β7-α5 connecting loop, which could have a direct influence on the PET binding and catalysis. In particular, we suggest that the rearrangement of this loop may be relevant for enabling the adoption of a proper conformation for PET recognition.

The comparison of PETase states analyzed in the FEL plots (Fig S10), revealed that the P1 (unbounded) and P4 (bounded) states demonstrate that the main change in the transition between the unbounded state to the bounded state is associated with β7-α5 connecting loop, which that exhibits movements of the residue Asp206 (see Fig S10). In P1 (Fig 5, PETase free), this residue interacts with His237 through hydrogen bond (1.78 Å) in PETase free. While the mobility of the β6-β7 connecting loop is associated mainly with the residue Trp185, which has a fluctuation in the change of states, while important catalytic residues, such as Trp159, Ser160, and His237 remain in stable conformations (see Fig 5C and Fig S11).

Conclusions

We have demonstrated a consistent model for simulating the PETase complexed with the PET, and its binding mode, which is in agreement with the currently available information in the literature. Our proposed model for PET binding mode can explain the conformational changes of protein structure and may be useful for the development of

new biocatalysts, as well as for the elucidation of the catalytic mechanism of plastic recycling enzymes. The determination of the binding mode of PET into the active site of PETase is important for understanding the catalytic mechanism of this enzyme. Our results also revealed that the β1-β2 connecting loop is very flexible and may be targeted for mutagenesis to increase the PETase stability. Overall, the results provide useful benchmarks for further engineering of PETase structure aiming the recycling of plastic polymers using this biological system.

Acknowledgments

Authors would like to thank the Laboratório Nacional de Computação Científica (LNCC) for providing access to the Santos Dumont Supercomputer for scientific calculations, and the Spanish Ministerio de Ciencia e Innovación (grant PGC2018-094852-B-C21), the Generalitat Valenciana (Grant AICO/2019/195) and Universitat Jaume I (grant UJI-B2020-03) for financial support. K.S and A.M.S are also grateful for the scholarship from the Brazilian funding agency Coordenação de Aperfeiçoamento de Pessoal de Nível Superior (CAPES, grant number: 88882.466102/2019-01 and 88887.599350/2021-00, respectively).

References

1. Restrepo-Flórez JM, Bassi A, Thompson MR. Microbial degradation and deterioration of polyethylene - A review. Int Biodeterior Biodegrad. 2014;88: 83–90. doi:10.1016/j.ibiod.2013.12.014

2. Brunner I, Fischer M, Rüthi J, Stierli B, Frey B. Ability of fungi isolated from plastic debris floating in the shoreline of a lake to degrade plastics. Aroca R, editor. PLoS One. 2018;13: e0202047. doi:10.1371/journal.pone.0202047

513 3. Jambeck JR, Geyer R, Wilcox C, Siegler TR, Perryman M, Andrady A, et al. Plastic
514 waste inputs from land into the ocean. Science (80-). 2015;347: 768–771.
515 doi:10.1126/science.1260352
516 4. Barnes DKA, Galgani F, Thompson RC, Barlaz M. Accumulation and fragmentation of
517 plastic debris in global environments. Philos Trans R Soc B Biol Sci. 2009;364: 1985–
518 1998. doi:10.1098/rstb.2008.0205
519 5. Picó Y, Barceló D. Analysis and prevention of microplastics pollution in water: Current
520 perspectives and future directions. ACS Omega. 2019;4: 6709–6719.
521 doi:10.1021/acsomega.9b00222
522 6. Yoshida S, Hiraga K, Takehana T, Taniguchi I, Yamaji H, Maeda Y, et al. A bacterium
523 that degrades and assimilates poly(ethylene terephthalate). Science (80-). 2016;351:
524 1196–1199. doi:10.1126/science.aad6359
525 7. Tournier V, Topham CM, Gilles A, David B, Folgoas C, Moya-Leclair E, et al. An
526 engineered PET depolymerase to break down and recycle plastic bottles. Nature.
527 2020;580: 216–219. doi:10.1038/s41586-020-2149-4
528 8. Chen Z, Wang Y, Cheng Y, Wang X, Tong S, Yang H, et al. Efficient biodegradation of
529 highly crystallized polyethylene terephthalate through cell surface display of bacterial
530 PETase. Sci Total Environ. 2020;709: 136138. doi:10.1016/j.scitotenv.2019.136138
531 9. Son HF, Cho IJ, Joo S, Seo H, Sagong H-Y, Choi SY, et al. Rational Protein
532 Engineering of Thermo-Stable PETase from Ideonella sakaiensis for Highly Efficient
533 PET Degradation. ACS Catal. 2019;9: 3519–3526. doi:10.1021/acscatal.9b00568
534 10. Taniguchi I, Yoshida S, Hiraga K, Miyamoto K, Kimura Y, Oda K. Biodegradation of
535 PET: Current Status and Application Aspects. ACS Catal. 2019;9: 4089–4105.
536 doi:10.1021/acscatal.8b05171
537 11. Tanasupawat S, Takehana T, Yoshida S, Hiraga K, Oda K. Ideonella sakaiensis sp. nov.,
538 isolated from a microbial consortium that degrades poly(ethylene terephthalate). Int J
539 Syst Evol Microbiol. 2016;66: 2813–2818. doi:10.1099/ijsem.0.001058
540 12. Palm GJ, Reisky L, Böttcher D, Müller H, Michels EAP, Walczak MC, et al. Structure

of the plastic-degrading Ideonella sakaiensis MHETase bound to a substrate. Nat Commun. 2019;10: 1717. doi:10.1038/s41467-019-09326-3

13. Joo S, Cho IJ, Seo H, Son HF, Sagong HY, Shin TJ, et al. Structural insight into molecular mechanism of poly(ethylene terephthalate) degradation. Nat Commun. 2018;9: 382. doi:10.1038/s41467-018-02881-1

14. Han X, Liu W, Huang JW, Ma J, Zheng Y, Ko TP, et al. Structural insight into catalytic mechanism of PET hydrolase. Nat Commun. 2017;8: 2106. doi:10.1038/s41467-017-02255-z

15. Fecker T, Galaz-Davison P, Engelberger F, Narui Y, Sotomayor M, Parra LP, et al. Active Site Flexibility as a Hallmark for Efficient PET Degradation by I. sakaiensis PETase. Biophys J. 2018;114: 1302–1312. doi:10.1016/j.bpj.2018.02.005

16. Dimarogona M, Nikolaivits E, Kanelli M, Christakopoulos P, Sandgren M, Topakas E. Structural and functional studies of a Fusarium oxysporum cutinase with polyethylene terephthalate modification potential. Biochim Biophys Acta - Gen Subj. 2015;1850: 2308–2317. doi:10.1016/j.bbagen.2015.08.009

17. Müller RJ, Schrader H, Profe J, Dresler K, Deckwer WD. Enzymatic degradation of poly(ethylene terephthalate): Rapid hydrolyse using a hydrolase from T. fusca. Macromol Rapid Commun. 2005;26: 1400–1405. doi:10.1002/marc.200500410

18. Nimchua T, Punnapayak H, Zimmermann W. Comparison of the hydrolysis of polyethylene terephthalate fibers by a hydrolase fromFusarium oxysporum LCH I andFusarium solani f. sp.pisi. Biotechnol J. 2007;2: 361–364. doi:10.1002/biot.200600095

19. Liebminger S, Eberl A, Sousa F, Heumann S, Fischer-Colbrie G, Cavaco-Paulo A, et al. Hydrolysis of PET and bis-(benzoyloxyethyl) terephthalate with a new polyesterase from Penicillium citrinum. Biocatal Biotransformation. 2007;25: 171–177. doi:10.1080/10242420701379734

20. Ribitsch D, Acero EH, Greimel K, Dellacher A, Zitzenbacher S, Marold A, et al. A new esterase from Thermobifida halotolerans hydrolyses polyethylene terephthalate (PET)

and polylactic acid (PLA). Polymers (Basel). 2012;4: 617–629. doi:10.3390/polym4010617

21. Sulaiman S, Yamato S, Kanaya E, Kim JJ, Koga Y, Takano K, et al. Isolation of a novel cutinase homolog with polyethylene terephthalate-degrading activity from leaf-branch compost by using a metagenomic approach. Appl Environ Microbiol. 2012;78: 1556–1562. doi:10.1128/AEM.06725-11

22. Herrero Acero E, Ribitsch D, Steinkellner G, Gruber K, Greimel K, Eiteljoerg I, et al. Enzymatic surface hydrolysis of PET: Effect of structural diversity on kinetic properties of cutinases from Thermobifida. Macromolecules. 2011;44: 4632–4640. doi:10.1021/ma200949p

23. Kitadokoro K, Thumarat U, Nakamura R, Nishimura K, Karatani H, Suzuki H, et al. Crystal structure of cutinase Est119 from Thermobifida alba AHK119 that can degrade modified polyethylene terephthalate at 1.76 Å resolution. Polym Degrad Stab. 2012;97: 771–775. doi:10.1016/j.polymdegradstab.2012.02.003

24. Austin HP, Allen MD, Donohoe BS, Rorrer NA, Kearns FL, Silveira RL, et al. Characterization and engineering of a plastic-degrading aromatic polyesterase. Proc Natl Acad Sci U S A. 2018;115: E4350–E4357. doi:10.1073/pnas.1718804115

25. Liu B, He L, Wang L, Li T, Li C, Liu H, et al. Protein crystallography and site-direct mutagenesis analysis of the poly(Ethylene terephthalate) hydrolase petase from Ideonella sakaiensis. ChemBioChem. 2018;19: 1471–1475. doi:10.1002/cbic.201800097

26. Billig S, Oeser T, Birkemeyer C, Zimmermann W. Hydrolysis of cyclic poly(ethylene terephthalate) trimers by a carboxylesterase from Thermobifida fusca KW3. Appl Microbiol Biotechnol. 2010;87: 1753–1764. doi:10.1007/s00253-010-2635-y

27. Roth C, Wei R, Oeser T, Then J, Föllner C, Zimmermann W, et al. Structural and functional studies on a thermostable polyethylene terephthalate degrading hydrolase from Thermobifida fusca. Appl Microbiol Biotechnol. 2014;98: 7815–7823. doi:10.1007/s00253-014-5672-0

28. Chen CC, Han X, Ko TP, Liu W, Guo RT. Structural studies reveal the molecular

597 mechanism of PETase. FEBS J. 2018;285: 3717–3723. doi:10.1111/febs.14612
598 29. Kawai F, Kawabata T, Oda M. Current knowledge on enzymatic PET degradation and
599 its possible application to waste stream management and other fields. Appl Microbiol
600 Biotechnol. 2019;103: 4253–4268. doi:10.1007/s00253-019-09717-y
601 30. Jones BJ, Lim HY, Huang J, Kazlauskas RJ. Comparison of Five Protein Engineering
602 Strategies for Stabilizing an α/β-Hydrolase. Biochemistry. 2017;56: 6521–6532.
603 doi:10.1021/acs.biochem.7b00571
604 31. Cui Y, Chen Y, Liu X, Dong S, Tian Y, Qiao Y, et al. Computational Redesign of a
605 PETase for Plastic Biodegradation under Ambient Condition by the GRAPE Strategy.
606 ACS Catal. 2021; 1340–1350. doi:10.1021/acscatal.0c05126
607 32. Trott O, Olson AJ. AutoDock Vina: Improving the speed and accuracy of docking with a
608 new scoring function, efficient optimization, and multithreading. J Comput Chem.
609 2009;31: NA-NA. doi:10.1002/jcc.21334
610 33. De Azevedo WFJ. MolDock applied to structure-based virtual screening. Curr Drug
611 Targets. 2010;11: 327–334. doi:10.2174/138945010790711941
612 34. Cole JC, Nissink JWM, Taylor R. Protein-ligand docking and virtual screening with
613 GOLD. Virtual Screening in Drug Discovery. 2005. pp. 379–415.
614 doi:10.1201/9781420028775.ch15
615 35. Case DA, Cheatham TE, Darden T, Gohlke H, Luo R, Merz KM, et al. The Amber
616 biomolecular simulation programs. J Comput Chem. 2005;26: 1668–1688.
617 doi:10.1002/jcc.20290
618 36. Li Y, Abberton BC, Kröger M, Liu WK. Challenges in multiscale modeling of polymer
619 dynamics. Polymers. 2013. pp. 751–832. doi:10.3390/polym5020751
620 37. Amari T, Ozaki Y. Generalized two-dimensional attenuated total reflection/infrared and
621 near-infrared correlation spectroscopy studies of real-time monitoring of the initial
622 oligomerization of bis(hydroxyethyl terephthalate). Macromolecules. 2002;35: 8020–
623 8028. doi:10.1021/ma020723y
624 38. Gartner TE, Jayaraman A. Modeling and Simulations of Polymers: A Roadmap.

Macromolecules. 2019. pp. 755–786. doi:10.1021/acs.macromol.8b01836

39. David CC, Jacobs DJ. Principal component analysis: A method for determining the essential dynamics of proteins. Methods Mol Biol. 2014;1084: 193–226. doi:10.1007/978-1-62703-658-0_11

40. Hornak V, Abel R, Okur A, Strockbine B, Roitberg A, Simmerling C. Comparison of multiple Amber force fields and development of improved protein backbone parameters. Proteins. 2006;65: 712–25. doi:10.1002/prot.21123

41. Frisch MJ. et. a., Nathan AJ, Scobell A. Gaussian 09. Gaussian, Inc. Wallingford CT. Wallingford CT: Gaussian Inc.; 2009. pp. 2–3. doi:111

42. Mark P, Nilsson L. Structure and Dynamics of the TIP3P, SPC, and SPC/E Water Models at 298 K. J Phys Chem A. 2001;105: 9954–9960. doi:10.1021/jp003020w

43. Gilson MK, Given JA, Bush BL, McCammon JA. The statistical-thermodynamic basis for computation of binding affinities: a critical review. Biophys J. 1997;72: 1047–69. doi:10.1016/S0006-3495(97)78756-

44. Roux B, Nina M, Pomès R, Smith JC. Thermodynamic stability of water molecules in the bacteriorhodopsin proton channel: a molecular dynamics free energy perturbation study. Biophys J. 1996;71: 670–81. doi:10.1016/S0006-3495(96)79267-6

45. Boresch S, Tettinger F, Leitgeb M, Karplus M. Absolute Binding Free Energies: A Quantitative Approach for Their Calculation. J Phys Chem B. 2003;107: 9535–9551. doi:10.1021/jp0217839

46. Mobley DL, Chodera JD, Dill KA. On the use of orientational restraints and symmetry corrections in alchemical free energy calculations. J Chem Phys. 2006;125: 084902. doi:10.1063/1.2221683

47. Palese LL. A random version of principal component analysis in data clustering. Comput Biol Chem. 2018;73: 57–64. doi:10.1016/j.compbiolchem.2018.01.009

48. Costa CHS, Oliveira ARS, dos Santos AM, da Costa KS, Lima AHL e., Alves CN, et al. Computational study of conformational changes in human 3-hydroxy-3-methylglutaryl coenzyme reductase induced by substrate binding. J Biomol Struct Dyn. 2019;37: 4374–

4383. doi:10.1080/07391102.2018.1549508

49. Costa CHS da, Bichara TW, Gomes GC, dos Santos AM, da Costa KS, Lima AHL e., et al. Unraveling the conformational dynamics of glycerol 3-phosphate dehydrogenase, a nicotinamide adenine dinucleotide-dependent enzyme of Leishmania mexicana. J Biomol Struct Dyn. 2020; 1–12. doi:10.1080/07391102.2020.1742206

50. Kumari P, Poddar R. A comparative multivariate analysis of nitrilase enzymes: An ensemble based computational approach. Comput Biol Chem. 2019;83: 107095. doi:10.1016/j.compbiolchem.2019.107095

51. Neves Cruz J, da Costa KS, de Carvalho TAA, de Alencar NAN. Measuring the structural impact of mutations on cytochrome P450 21A2, the major steroid 21-hydroxylase related to congenital adrenal hyperplasia. J Biomol Struct Dyn. 2020;38: 1425–1434. doi:10.1080/07391102.2019.1607560

52. Li C, Chen S, Huang T, Zhang F, Yuan J, Chang H, et al. Conformational Changes of Glutamine 5′-Phosphoribosylpyrophosphate Amidotransferase for Two Substrates Analogue Binding: Insight from Conventional Molecular Dynamics and Accelerated Molecular Dynamics Simulations. Front Chem. 2021;9. doi:10.3389/fchem.2021.640994

53. Valente RP da P, Souza RC de, de Medeiros Muniz G, Ferreira JEV, de Miranda RM, e Lima AHL, et al. Using Accelerated Molecular Dynamics Simulation to elucidate the effects of the T198F mutation on the molecular flexibility of the West Nile virus envelope protein. Sci Rep. 2020;10: 9625. doi:10.1038/s41598-020-66344-8

54. Grosso M, Kalstein A, Parisi G, Roitberg AE, Fernandez-Alberti S. On the analysis and comparison of conformer-specific essential dynamics upon ligand binding to a protein. J Chem Phys. 2015;142: 245101. doi:10.1063/1.4922925

55. Salmas RE, Yurtsever M, Durdagi S. Investigation of Inhibition Mechanism of Chemokine Receptor CCR5 by Micro-second Molecular Dynamics Simulations. Sci Rep. 2015;5: 13180. doi:10.1038/srep13180

56. Liu Y, Chipot C, Shao X, Cai W. Edge effects control helical wrapping of carbon nanotubes by polysaccharides. Nanoscale. 2012;4: 2584–2589. doi:10.1039/c2nr11979j

57. Grant BJ, Rodrigues APCC, ElSawy KM, McCammon JA, Caves LSDD. Bio3d: An R package for the comparative analysis of protein structures. Bioinformatics. 2006;22: 2695–2696. doi:10.1093/bioinformatics/btl461

58. Karamzadeh R, Karimi-Jafari MH, Sharifi-Zarchi A, Chitsaz H, Salekdeh GH, Moosavi-Movahedi AA. Machine Learning and Network Analysis of Molecular Dynamics Trajectories Reveal Two Chains of Red/Ox-specific Residue Interactions in Human Protein Disulfide Isomerase. Sci Rep. 2017;7: 3666. doi:10.1038/s41598-017-03966-5

59. Papaleo E, Mereghetti P, Fantucci P, Grandori R, De Gioia L. Free-energy landscape, principal component analysis, and structural clustering to identify representative conformations from molecular dynamics simulations: The myoglobin case. J Mol Graph Model. 2009;27: 889–899. doi:10.1016/j.jmgm.2009.01.006

60. Ma Y, Yao M, Li B, Ding M, He B, Chen S, et al. Enhanced Poly(ethylene terephthalate) Hydrolase Activity by Protein Engineering. Engineering. 2018;4: 888–893. doi:10.1016/j.eng.2018.09.007

61. Knott BC, Erickson E, Allen MD, Gado JE, Graham R, Kearns FL, et al. Characterization and engineering of a two-enzyme system for plastics depolymerization. Proc Natl Acad Sci. 2020;117: 25476–25485. doi:10.1073/pnas.2006753117